J. Appl. Cryst. (1995). **28**, 717–728

Approximations Leading to a Unified Exponential/Power-Law Approach to Small-Angle Scattering

BY G. BEAUCAGE

Department of Materials Science and Engineering, University of Cincinnati, Cincinnati, OH 45221-0012, *USA*

(*Received* 11 *December* 1994; *accepted* 24 *May* 1995)

Abstract

A new approach to the analysis of small-angle scattering is presented that describes scattering from complex systems that contain multiple levels of related structural features. For example, a mass fractal such as a polymer coil contains two structural levels, the overall radius of gyration and the substructural persistence length. One structural level is described by a Guinier and an associated power-law regime. A function is derived that models both the Guinier exponential and structurally limited power-law regimes without introducing new parameters beyond those used in local fits. Account is made for both a low-q and a high-q limit to power-law scattering regimes. The unified approach can distinguish Guinier regimes buried between two power-law regimes. It is applicable to a wide variety of systems. Fits to data containing multiple power-law and exponential regimes using this approach have previously been reported. Here, arguments leading to the unified approach are given. The usefulness of this approach is demonstrated through comparison with model calculations using the Debye equation for polymer coils (mass fractal), equations for polydisperse spheres (Porod scattering) and randomly oriented ellipsoids of revolution with diffuse interfaces, as well as randomly oriented rod and disc-shaped particles.

1. Introduction

Recent developments concerning the fractal analysis of power-law behavior in small-angle scattering (Schmidt, 1992; Korberstein, Morra & Stein, 1980; Debye, Henderson & Brumberger, 1957; Fischer & Burford, 1967) have made it evident that a number of materials display at least two observable power-law scaling regimes (Fig. 1). Experimentally observed power-law regimes display structural limits at both high and low q. These limits are manifested as regimes of exponential decay in scattering following Guinier's law. This behavior has been interpreted as reflecting interfacial or mass-fractal scattering from a large-scale structure in the low-q power-law regime composed of small-scale substructures whose mass-fractal or surface-fractal scaling is observed in the high-q power-law regime. The region of exponential decay between the two power laws reflects the average size of the substructural particles.

Recently, we have been able to obtain scattering data that span an extremely large size range from 10 μm to 5 Å using light scattering and absolute intensity measurements from a Bonse–Hart X-ray camera,* a conventional pinhole small-angle X-ray scattering (SAXS) camera† and an X-ray diffractometer. Some of these data display two discrete exponential regimes and two discrete power-law regimes. Fig. 1 shows an example of such combined data for a polyacrylonitrile. (PAN) low-density foam made by R. Lagasse. Two size scales of structure and two regimes of constant mass/size scaling are observed. The 'knees' in the log–log plot reflect regions of exponential decay in scattered intensity that correspond to an average structural size according to Guinier's law in exponential form. The power-law regions reflect constant mass scaling with size of measurement according to the various mass- or surface-fractal scattering laws. These power-law regimes are limited at each end by structural limits to this scaling behavior. A Guinier regime and its corresponding power-law regime are here termed one 'structural level'. It is possible to fit these regimes separately using two power-law functions and two exponential functions. Often, an intermediate exponential regime ($q = 4 \times 10^{-2}$ Å^{-1} in Fig. 1) is obscured owing to extensive overlap with two neighboring power-law regimes. Additionally, one is often left with few data solely pertaining to the power-law regimes, owing to instrumental limitations, weak statistics, background scattering and the interference of diffraction at very high values of q.

By consideration of the structural limits at both the high- and low-q extremes in the development of equations describing power-law scattering, a unified expression that describes exponential and power-law scattering, as well as multiple structural levels in small-

* National Institute of Standards and Technology beamline at Brookhaven National Laboratories National Synchrotron Light Source; G. Long, D. Fischer.

† 10 m small-angle X-ray camera at Oak Ridge National Laboratory; J. S. Lin.

angle scattering, has been developed. This new expression has been shown to be extremely useful in globally analyzing data sets such as that shown in Fig. 1 (Beaucage & Schaefer, 1994; Beaucage, Ulibarri, Black & Schaefer, 1994; Ulibarri, Beaucage, Schaefer, Olivier & Assink, 1992; Hua, Anderson, Hareid, Smith & Beaucage, 1994). Although several authors have presented semi-empirical functions that are able to fit length-scale-limited power-law scattering for specific types of mass scaling, none are adequate over five decades in size (Lin, Klein, Lindsay, Weitz, Ball & Meakin, 1990; Schaefer & Hurd, 1990; Wiltzius, Bates, Dierker & Wignall, 1987; Mountain & Mulholland, 1988; Mountain, Mulholland & Baum, 1986; Hurd, 1990). The unified approach presented here, on the other hand, is amenable to any type of power-law scattering and is capable of describing scattering functions containing multiple structural levels.

The unified exponential/power-law approach describes scattering data, such as those shown in Fig. 1, over several structural levels without introducing additional parameters beyond the number used in local Guinier and power-law fits. It can also be used to duplicate calculated scattering curves for polydisperse spheres, ellipsoids of revolution, Debye polymer coils, mass fractals of arbitrary dimension and randomly oriented rod and lamellar particulates. Local and global fits agree well with improved resolution for data fits using the unified approach because more data points are used and because account is made for overlapping features in the scattering pattern. Additionally, use of the unified approach clarifies the limits to power-law and Guinier-exponential scattering, thereby removing uncertainty as to the appropriate fit range for these functional forms.

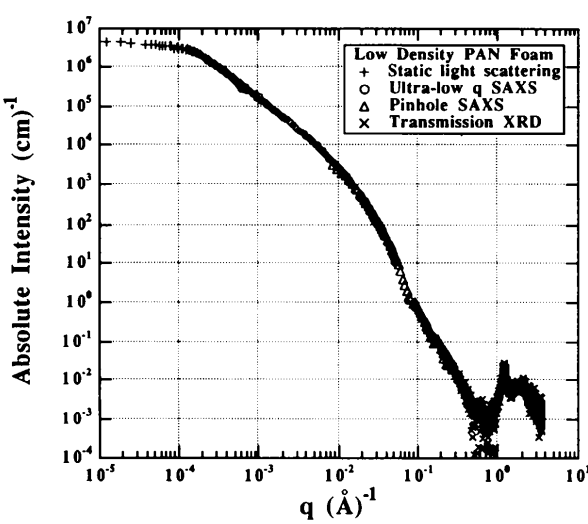

Fig. 1. Log–log plot of combined small-angle scattering data from a low-density polymer foam (obtained from R. Lagasse). + light scattering from foam imbibed with an index-matching solvent; ○ Bonse–Hart data (see footnote to text); △ conventional pinhole X-ray scattering data (see footnote to text); × X-ray diffraction (XRD) data. The data spans sizes from 10 μm to 5 Å. The peaks in the data at high q are due to diffraction and the amorphous halo of the polymer.

2. Correlation function, Guinier's law and power laws

A particulate structure is considered in the development of a unified scattering function. The final equations are general in application to nonparticulate systems (Beaucage & Schaefer, 1994; Beaucage, Ulibarri, Black & Schaefer, 1994; Ulibarri, Beaucage, Schaefer, Olivier & Assink, 1992; Hua, Anderson, Hareid, Smith & Beaucage, 1994). Parallel derivations are possible for these systems. In §8, it is demonstrated that the approach can approximate scattering from mass fractals such as polymer coils, surface fractals and diffuse interfacial structures.

Porod (1951, 1952) introduced the characteristic function $\gamma(r)$ or correlation function, which, in a particulate system, represents the probability that a point at a radial distance r from a given point in a particle phase will also be in the particle phase. $\gamma(r)$ is related to the form factor by

$$\overline{F^2(\mathbf{q})} = V_p \rho_e^2 \int_0^\infty \int_0^\infty \int_0^\infty \gamma(r) \exp(-i\mathbf{q}\cdot\mathbf{r})\, d\mathbf{r}, \qquad (1)$$

where V_p is the volume of a particle and ρ_e is the particle's electron density. $\mathbf{q}$ is a vector describing the difference between the incident and scattered beams. Its magnitude is $(4\pi/\lambda)\sin(\theta/2)$, where θ is the scattering angle. The scattered intensity and the correlation function are related by a Fourier transform. In order to account for concentrated particles, ρ_e^2 in (1) can be replaced by $\langle\eta^2\rangle = \varphi_p(1-\varphi_p)(\rho_p - \rho_0)^2$, where φ_p is the volume fraction of particles and ρ_0 is the electron density of the surroundings of the particles.

A simplified description of the form factor was derived by Debye for the case of centrosymmetric particles that are rotationally averaged (Debye, 1915; Guinier & Fournet, 1955, p. 12):

$$\overline{F^2(q)} = V_p \rho_e^2 \int_0^\infty \gamma(r)[\sin(qr)/qr] 4\pi r^2\, dr. \qquad (2)$$

In (2), the function $\sin(qr)/qr$ serves to weight the product $r^2\gamma(r)$ by a radially symmetric phase factor involving the product of q and r, $w(q, r) = \sin(qr)/qr$. The product $r^2\gamma(r)$ is termed the distance distribution function, $p(r)$.

The correlation function, $\gamma(r)$, can be calculated exactly only for extremely simple structures. For a sphere,*

$$\gamma_{\text{sphere}}(r) = 1 - (3r/4R) + (1/16)(r/R)^3, \qquad (3)$$

where R is the radius of the sphere.

*A number of references are found for (3). The original derivation is probably due to Porod (Guinier & Fournet, 1955, p. 15; Feigin & Svergun, 1987, p. 42).

The aim here is to obtain a general expression that can continuously describe both the low-q Guinier regime and a related high-q power-law regime for the same particle. We can consider general features of (2) to understand the difference between these two regimes, using Porod's law as an example of a power-law regime and a Fourier transform of Guinier's law for the Guinier regime. These are compared to the correlation function for a sphere, (3).

The equivalent of a correlation function for Guinier's law can be obtained by Fourier transformation of Guinier's law. This leads to a Gaussian function:

$$\gamma_{\text{Gaussian}}(r) = \exp(-3r^2/4R_g^2). \tag{4}$$

For a sphere, this becomes

$$\gamma_{\text{Gaussian sphere}}(r) = \exp(-5r^2/4R^2), \tag{5}$$

where R is the radius of the sphere and R_g^2 for the sphere is given by $\frac{3}{5}R^2$.

For Porod's law, the local correlation function is approximated by (Guinier & Fournet, 1955, p. 15)

$$\gamma_{\text{Porod}}(r) = 1 - (Sr/4V), \tag{6}$$

where S is the particle's surface area and V is the particle's volume. For a sphere, (6) becomes

$$\gamma_{\text{Porod sphere}}(r) = 1 - (3r/4R). \tag{7}$$

Fig. 2 compares the sin $(qr)/qr$ weighting function of (2), $w(q, r)$, at several values of q with the three correlation functions described by (3), (5) and (7) using $R_{\text{sphere}} = 80$ Å. Fig. 2 is presented to note several general features of the correlation functions so that the limitations of power-law and Guinier scattering can be understood. At low q, $w(q, r)$ is approximately constant and has a value close to 1 over the range where $\gamma(r)$ has nonzero values. This means that low-q scattering is described by the integral of $4\pi\gamma(r)r^2$. This is equal to the average particulate volume, V_p (Guinier & Fournet, 1955, p. 13). [In (2), the integral is multiplied by V_p so that the intensity depends on $V_p^2 q$.] At high q, the weighting function shows large values and asymmetry about 0 only for the first few oscillations at small values of r. $w(q, r) = 0$ at $r = \pi/q$, $2\pi/q$ *etc.*, so that only values of r less than $2\pi/q$ are important to the high-q intensity. $\gamma_{\text{Porod}}(r)$ closely matches the exact function for a sphere of radius 80 Å with a sharp interface for r less than about 40 Å. This is improved to about 50 Å in the comparison of $4\pi r^2\gamma(r)$ shown in Fig. 3. The first derivative of the correlation function is $S/4V$ (Feigin & Svergun, 1987, p. 43). For the Gaussian function at small r, this is 0. This means that the Gaussian function describes a particle with no surface.

Fig. 3 compares $4\pi r^2\gamma(r)$ for the three cases of (3), (5) and (7). From Figs. 2 and 3, it is clear that a local description of the structure is completely lacking in the Gaussian function. The importance of this function is that an integral of $\gamma(r)$ and $4\pi r^2\gamma(r)$ over r for the Gaussian function approximates the exact integrals for the sphere to about 95% accuracy. These integrals are equal to half the correlation length, $\bar{l}/2$, and the average particle volume, $\bar{V}_p$, respectively. It is the particle averaged in orientation and position that is described by the Gaussian function, (4), and Guinier's law. Integrals of the Gaussian function weighted by $w(q, r)$ also give about 95% of the exact value. Integrals of the Gaussian function deviate from the exact value because local structural features are not considered. In contrast to this, integrals for power-law correlation functions do not approximate the average

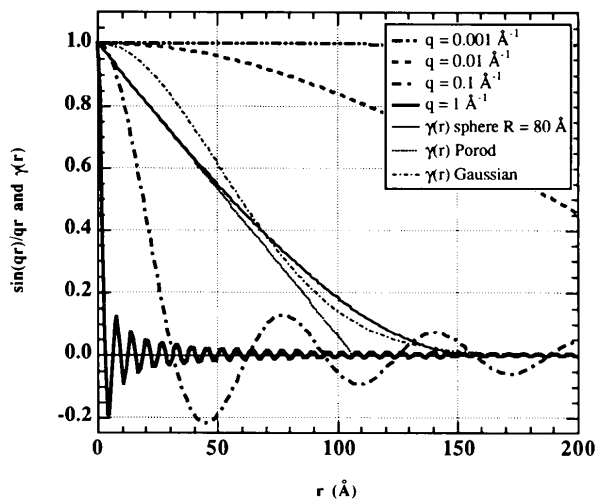

Fig. 2. The weighting factor, sin $(qr)/qr$ for several values of q and the correlation functions from equations (3), (5) and (7) using $R = 80$ Å as a function of r.

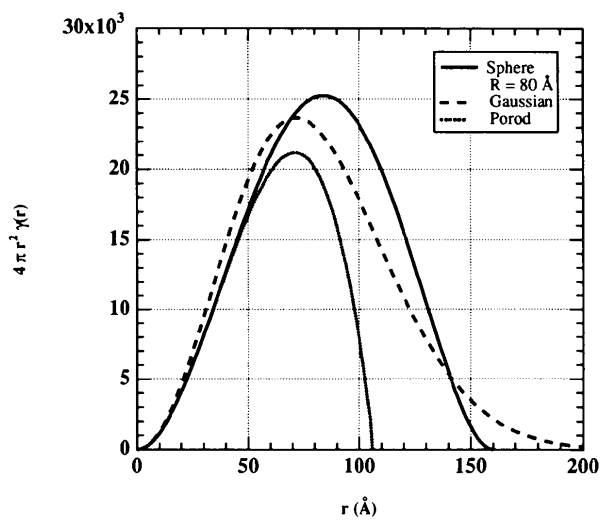

Fig. 3. Comparison of $4\pi r^2\gamma(r)$ as a function of r for equations (3), (5) and (7).

(integral) particle features, while the local (differential) features are closely matched.

The Gaussian excludes a description of local features, such as surface or mass-fractal scaling, that are described by power laws such as Porod's law. In this paper, limits to power laws are obtained that exclude conditions where the average particle features become important. After such limitations, power laws and Guinier's exponential form can be viewed, to a good approximation, as independent sources of scattering, and can be summed to yield a unified equation.

3. Derivation of Guinier's law

From the discussion above, it can be said that Guinier's law is the Fourier transform of the correlation function for a particle randomly averaged about its orientation and its position relative to the scattering reference frame. As noted above, the correlation function, $\gamma(r)$, is defined by the probability that a point at a radial distance r from a given point in a particle phase will also be in the particle phase. First, a particle randomly averaged with respect to the scattering reference frame is considered. (Fig. 4). Random positioning of the scattering reference frame about the particle structure leads to an average structure described by a radially symmetric probability function. This function contains only information concerning the average properties of the particle such as the correlation length and the volume. Information concerning local structure such as a description of the surface is completely lost in this averaging.*

Random placement of the initial point and orientation of the vector $\mathbf{r}$ is analogous to fixing the initial point of $\mathbf{r}$ and allowing the particle to randomly diffuse about this point. The initial point remains in the particle, so diffusion from 0 to r_{max}, the maximum particulate dimension, is allowed. After such a randomization process, the probability of finding a point in the particle at a distance r from the initial point is given by a Gaussian function whose value is 1 at $r=0$ owing to the constraint that the origin of $\mathbf{r}$ remains in the particle. Because of the averaging of structure, there is no possibility of accounting for the particulate surface or other local features in this description.

The correlation function for such an averaged particle is described in real space by a three-dimensional Gaussian function, fixed at unit probability for $r=0$:

$$\gamma_{\text{Gaussian}}(r) = \exp(-3r^2/2\sigma^2). \tag{8}$$

σ^2 is the variance of the distribution that is described as the average of the square of the deviations of vectors describing particle position, $\mathbf{x}_i$, from a vector, $\boldsymbol{\mu}$, describing the origin of the vector $\mathbf{r}$,

$$\sigma^2 = \left[\sum_{i=1}^{N}(\mathbf{x}_i - \boldsymbol{\mu})^2\right] \Big/ N, \tag{9}$$

where N is the total number of particle positions considered.

For the case of the Guinier regime, a double sum is carried out to obtain the variance, σ^2. As noted above, the vector $\boldsymbol{\mu}$ in (9) is the origin for the vector $\mathbf{r}$. Translations of the particle are randomly distributed about this origin. For consideration of any possible origin, a summation over any initial point in a particle must be carried out, one summation in (10). This is analogous to considering an average particle position relative to the experimental frame of reference for the particulate suspension. The second summation, (9) and (10), pertains to the summation of all points in this average particle relative to the origin of $\mathbf{r}$.

$$\sigma^2_{\text{Guinier}} = \sum_l \sum_{m \neq l} f_l f_m (\mathbf{r}_{lm})^2 \Big/ \sum_l \sum_{m \neq l} f_l f_m = 2R_g^2. \tag{10}$$

l and m are indexes for scattering points, $\mathbf{r}_{lm}$ is a vector separating two points in an average particle and f_l is the scattering factor for point l in the particle. As shown in (10), the variance for the Guinier regime is defined by $2R_g^2$.

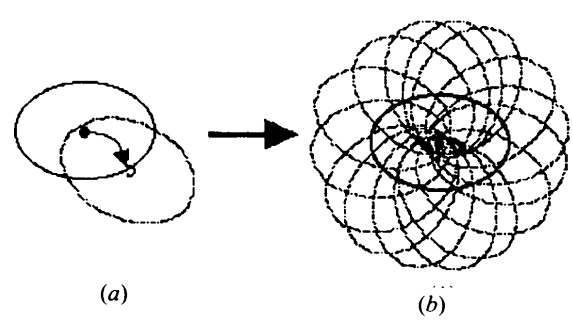

(a) (b)

Fig. 4. Averaging of a particle about the origin of the vector $\mathbf{r}$ in analogy to random translations and rotations of the particle about the origin of $\mathbf{r}$. In (*a*), a single rotation and a single translation are considered. In (*b*), the superposition of a number of such translations and rotations in random directions leads to a Gaussian distribution of scattering density $\rho(r)$.

* For a sphere, (3), it was noted that an exact correlation function can be obtained by averaging over the position and orientation of a pair of scattering elements. This procedure leads to a correlation function that contains information about the sphere surface. Guinier & Fournet (1955, pp. 15–18), calculate (3) following the approach of overlapping volumes of Wilson (1949), where $\gamma(r) = \langle V(r)\rangle / V$, $\langle V(r)\rangle$ is the volume common in two spheres of radius R whose centers are separated by r and V is the sphere volume. With this approach, $\gamma(r)$ is zero when r is greater than R. Thus, (3) includes a description of the surface of the sphere. This should be contrasted with the exponential function, (8) and (11), describing an average particle (Fig. 4). $\gamma(r)$ in this case does not have a sharp limit at finite particle dimensions. This is because there is not a well defined value of r in the averaged particle of Fig. 4 where the particle ends. A finite probability exists up to the maximum particle dimension, which is reflected in the correlation function only through the average radius [(11)]. At small r, the sphere correlation function, (3), displays linear behavior in r owing to this description of the surface. The exponential function, if expanded, does not have a term linear in r at small r. As noted in the text, it is the prefactor to this linear term that describes a finite particle surface area (Feigin & Svergun, 1987, p. 47).

For the Guinier regime, the correlation function, $\gamma(r)_{\text{Guinier}}$ fixed at unit probability for $r=0$, is

$$\gamma(r)_{\text{Guinier}} = \exp(-3r^2/4R_g^2). \quad (11)$$

This can be Fourier transformed according to (1) to yield Guinier's exponential form,

$$I(q) = I_e \overline{N_p} n^2 \exp(-R_g^2 q^2/3). \quad (12)$$

$\overline{N_p}$ is the number of particles in the scattering volume, I_e is the scattering factor for a single electron and n is the number of electrons in a particle.

4. Structurally limited power laws

The correlation functions for power laws such as Porod's law are good descriptions of the local structure (Figs. 2 and 3). They fail to describe integral properties such as the correlation length or the particle volume. To describe scattering from both the integral structure, as described by the Gaussian function, and the local structure, as described by power-law descriptions, a limit to the local description is needed. This limit describes the diminution of power-law contributions to the total scattered intensity owing to the average particle structure (Figs. 5 and 6). This diminution will occur on decreasing q and will serve as a low-q cut-off for power-law scattering. When this diminution is properly accounted for, in the same terms as used in the derivation of the Gaussian function, a low-q limited power law can be summed with Guinier's law to yield a description of both the Guinier regime and the power-law regime for one structural level. As noted above, Guinier's law does not account for local structure, so it can be used in this sum without modification.

In the derivation of power-law scattering equations such as Porod's law for a particulate system, the particle is divided into two regions that will be termed the Porod surface and the Porod bulk (Fig. 5). The dominant effects are related to small sizes, where the surface of an arbitrarily shaped particle can be considered locally flat (Fig. 5*a*). The vectors '**r**' in Fig. 5 are shown in various orientations indicating rotational averaging of **r** in the derivation of Porod's law. The origin of **r** is placed at random in the particle.

As noted above, Porod scattering considers a sharp locally flat interface. The Porod surface is a region partially excluded from the correlation function, $\gamma(r)$ (Porod, 1982, p. 30). The correlation function, in the derivation of Porod's law, is obtained from geometric consideration of the contributions to scattering from the Porod bulk and half of the Porod surface (Porod, 1982, p. 30). With this condition, a functional form for $\gamma(r)$ is derived (Guinier & Fournet, 1955, pp. 14–15) for a sharp planar interface as shown in Fig. 5(*a*):

$$\gamma(r) = 1 - (S/4V)r + \ldots, \quad (13)$$

where S/V is the surface-to-volume ratio for the particle. The Porod correlation function is described as the probability that two points separated by a distance r in an arbitrary direction will be in the Porod bulk or in the inner half of the Porod surface. This is here termed the 'Porod condition'. Large-size structural features of the particle, such as the radius of gyration, are ignored in (13). Integration of (2) using (13) leads to an expression, the nonoscillating terms of which have a q^{-4} dependence:

$$\overline{F^2(q)} \simeq 2\pi\rho_e^2 S/q^4. \quad (14)$$

Oscillating terms are considered to average to zero at high q, especially for nonspherical particles.

Equation (14) yields an excess of scattered intensity below $q \simeq 2\pi/R_g$. This is because the structural model shown in Fig. 5(*a*) fails at small values of q or large $|\mathbf{r}|$ as shown in Fig. 5(*b*). In Fig. 5(*b*), the terminal points of the left and right vectors of Fig. 5(*a*) do not meet the Porod condition owing to finite limits of the particle. Porod's law erroneously considers the left vector as contributing to scattering. This leads to an overestimation of the scattered intensity at low q. For large 'r', the Porod

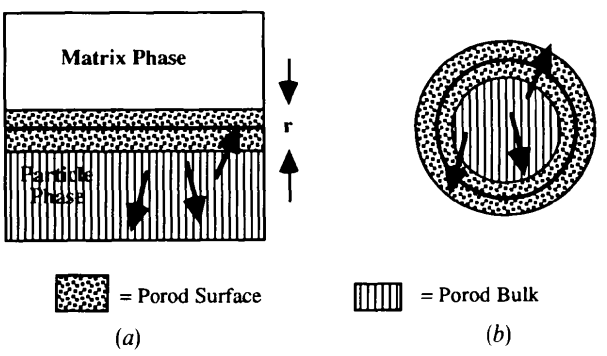

Fig. 5. (*a*) Classic Porod scattering and (*b*) structurally limited Porod scattering. The bold arrows in the figure represent $(\mathbf{r}_m - \mathbf{r}_l)$ for arbitrary pairs of points in the particle. Variation in direction of this vector indicates rotational averaging of **r** in the derivation of Porod's law (see footnote to text). The internal half of the Porod surface and the Porod bulk contribute to scattering (Guinier & Fournet, 1955, pp. 14–15).

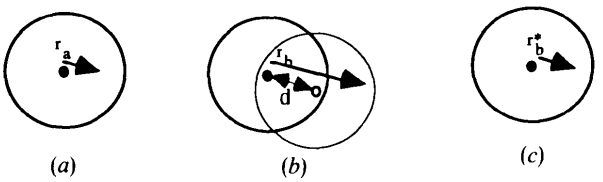

Fig. 6. A particle with center of mass at the solid dot. The arrow connects two points separated by 'r'. In (*b*), 'r' is larger than in (*a*), leading to a loss of the Porod condition. In (*c*), r_b^* has some probability of describing the random placement of the initial point of the vector **r** as described in the text. $r_b^* = r_b - d = r_a$. The particles shown are composed of the Porod bulk plus the inner half of the Porod surface (Guinier & Fournet, 1955, pp. 14–15).

surface encompasses most of the particle. This will lead to a dramatic decrease in the contribution of power-law scattering to the total scattered intensity.

A centrosymmetric particle is considered containing two points randomly placed in the particle (meeting the Porod condition) and separated by the vector **r**, whose absolute value is close to r_{max}, the maximum particle dimension in the direction of **r**. The two points are connected by an arrow in Fig. 6. The particle shown in Fig. 6 is composed of the Porod bulk and the inner half of the Porod surface (Porod, 1982, p. 30). As $|\mathbf{r}|$ becomes larger, it approaches the particle size (Fig. 6*b*), leading, in some cases, to the loss of the Porod condition. Random placement of the origin of **r** relative to the particle structure has some probability of leading to the Porod condition (Fig. 6*b*). In analogy to the development of the Gaussian correlation function, this random placement can be described by a Gaussian function. This might result from Brownian diffusion of the particle about a fixed experimental reference frame (double arrow in Fig. 6). In the derivation of Porod's law, the probability for a displacement parallel to the surface in Fig. 5(*a*) and leading to the Porod condition is 1, regardless of the particle shape or the length of *r*. Here, this Gaussian function will be less than 1 for *r* close to r_{max}.

The probabilistic description of the random location of the origin of the vector **r** can be thought to reduce '*r*' by a factor that is related to the average particle dimension and the size of *r* as shown in Fig. 6(*c*), where $r_b^* = r_b - d = r_a$. Fig. 6(*a*) shows a vector **r** for which the Porod approach might be appropriate. In Fig. 6(*b*), the vector **r** is close to r_{max} in length. Because the particle is finite, this vector bridges the particle boundary and does not contribute to scattering. Translation of the initial point for the vector or an equivalent translation of the particle brings both ends of the vector into the particle phase. It is the probability of random placement of **r** leading to this condition that is considered. This must modify the correlation function. If the original starting position is retained, this particulate translation can be viewed as effectively reducing the length of the vector **r** (Fig. 6*c*). Since *r* and *q* are Fourier equivalents, a reduction in *r* can be considered in terms of an equivalent increase in *q*. It is the maximum dimension of the particle, r_{max}, that leads to the loss of some possibilities for the Porod condition and to decay in the power-law contribution to the intensity near R_g.

To account for finite structural effects in power laws, a factor that modifies *q* to a reduced q^* will be obtained. Beyond an average particle size, q^* becomes rapidly larger as *q* becomes smaller. This serves to 'cut off' the power law at low *q*. By substitution of the reduced parameter q^* for *q*, conventional derivations of power-law scattering equations can be retained, as described below. The random placement of the origin of the vector **r** will be described in analogy to random diffusion of the particle about a fixed origin.

The probability for the condition of Figs. 6(*b*) and (*c*) is considered. As noted above, this probability factor will modify the correlation function in (2) [as defined by (13) for example], accounting for the effect of finite particle size on the correlation function. Superimposed on the reference frame of **r**, three-dimensional Brownian diffusion (in analogy to random placement of the origin of **r**) is allowed to occur so that the particle has a component of its displacement parallel to **r** and this component has a placement distance '*d*' (Fig. 6*b*). A probability function accounts for the probability of a translation of the particle along **r** a distance '*d*' resulting in both ends of the vector **r** meeting the Porod conditions. This probability is erroneously assumed to be 1 for Porod's law. As in the derivation of Guinier's exponential form, above, this Brownian diffusion (random placement) is described by a Gaussian,

$$p(r)_{1-d} = k \exp(-3r^2/2\sigma^2), \tag{15}$$

where *k* accounts for the probability of random diffusion occurring in the positive direction of **r**. Equation (15) is a three-dimensional Gaussian because Brownian diffusion occurs in three dimensions. It is a one-dimensional probability because only one orientation of the vector **r** has been considered.

Equation (15) is converted to *q* space through a Fourier transform because we are interested in a factor that modifies $|\mathbf{q}|$. This yields

$$p(q)_{1-d} = k \exp(-q^2\sigma^2/6). \tag{16}$$

The variance, σ^2, in (16) is defined by (9), $\sigma^2 = \sum_{i=1}^{N}(\mathbf{x}_i - \boldsymbol{\mu})^2/N$. Here, $\boldsymbol{\mu}$ is a vector describing the particle's center of mass. This ensures that translations lead to the Porod condition for the origin of **r**. This also accounts for the independent orientational averaging of **r** in the development of Porod's law. The summation over $\mathbf{x}_i$, in (9), accounts for displacement of the particle a distance '*d*' (Fig. 6). If the origin for the vector **r** is at the center of mass, the maximum displacement is a distance $r_{max}/2$ for a centrosymmetric particle, or, for a sphere, the radius of the sphere. Here, r_{max} is the maximum particulate dimension in the direction of **r**. Setting the initial position of **r** at the center of mass and limiting translations to $r_{max}/2$ ensures the Porod condition for the origin of the vector **r**.

To account for all possible distances '*d*' that lead to the Porod condition, a summation of (16) over spheres of radius $d=0$ to $d=r_{max}/2$ is necessary. That is a summation over σ from $\sigma=0$ to $\sigma=\sigma_{max}$.

$$\overline{p(q)_{1-d}} = (2/\pi^{1/2}) \int_{w=0}^{Y} \exp(-w^2)\,dw, \tag{17}$$

where $Y = q\sigma_{max}/6^{1/2}$. Equation (17) has been normalized. For an arbitrarily shaped centrosymmetric particle,

σ_{max} is defined by

$$\sigma_{max}^2 = \sum_k f_k |\mathbf{OM}_k|^2 \Big/ \sum_k f_k = R_g^2, \qquad (18)$$

where f_k is the scattering factor for point k and $\mathbf{OM}_k$ is the vector from the center of mass of an average particle to a point k. The maximum value for σ accounts for all points that could lead to the Porod condition in an average particle.

Equation (18) describes a one-dimensional probability due to finite structure as the error function of Y,

$$\overline{p(q)_{1-d}} = \text{erf}\,(qR_g/6^{1/2}). \qquad (19)$$

As noted above, this is a one-dimensional probability because only one orientation of $\mathbf{r}$ with respect to the particle's local frame of reference (the surface for Porod's law) was considered. To consider other orientations of the particle with respect to $\mathbf{r}$, the one-dimensional probability function is cubed. This describes a three-dimensional probability function, $p(q, R_g)$, assuming that the other two dimensions are equivalent and can be considered independently.

$$p(q, R_g) = [\text{erf}\,(qR_g/6^{1/2})]^3. \qquad (20)$$

Equation (20) modifies the correlation function, $\gamma(r)$, in (2) by accounting for the probability that the Porod or other power-law correlation functions meet the conditions discussed for a particle with finite structure. A useful approximation to this correction is to substitute the reduced parameter q^* for q in (2), where q^* is given by

$$q^* = q/[\text{erf}\,(qR_g/6^{1/2})]^3. \qquad (21)$$

Modification of q allows for simple modification of power laws to account for finite structure. In this way, (2) is rewritten

$$\overline{F^2(q)} = V_p\rho_e^2 \int_0^\infty \gamma(r)[\sin(qr)/q^*r]4\pi r^2\, dr$$

$$\simeq V_p\rho_e^2 \int_0^\infty \gamma(r)[\sin(q^*r)/q^*r]4\pi r^2\, dr, \qquad (22)$$

where the first term is the exact expression and the second is the approximation of substituting q^* for q.

A structurally limited Porod's law is given by

$$\overline{F^2(q)} \simeq 2\pi\rho_e^2 S/q^{*4} = 2\pi\rho_e^2 S\{[\text{erf}\,(qR_g/6^{1/2})]^3/q\}^4. \qquad (23)$$

The approximation in (22) is exact for high q, where the original form of the weighting function, $w(q, r) = \sin(qr)/qr$, is identical to the approximation $\sin(q^*r)/q^*r$ and to the properly corrected function $\sin(qr)/q^*r$. For q above $2\pi/R_g$, the approximation of (22) is very good. For low q, the approximation is also good, as shown in Fig. 7. This is because both the approximated and correct functions lead to very small scattered intensities at low q compared with Guinier's law. Between $q = \pi/R_g$ and $2\pi/R_g$, the approximation of (22) leads to a steeper decay in the integral of (2) than is predicted by the correct function. In application, errors due to this approximation are not observed for surface fractal or diffuse interfaced systems where the power-law decay in scattered intensity is steeper than -3. For systems displaying weak power-law decays in intensity, the approximation leads to a slight depletion in scattered intensity between $q = \pi/R_g$ and $2\pi/R_g$. In the example of a Debye polymer coil given in §8 (Fig. 10), this weak depletion is demonstrated. Empirical corrections for this approximation are possible, such as a constant shift factor for R_g in the error function term. These are generally not necessary since even with this approximation the value for least-squares fits, to the Debye equation for example, are within 95% of the exact values.

Fig. 8 shows plots of q^* *versus* q and $1/q^*$ demonstrating the difference between the reduced q^* and q. The $1/q$ plot parallels the limiting behavior on $|\mathbf{r}|$ near R_g as $|\mathbf{r}|$ is increased. Equivalent values of $1/q^*$ before and after the peak are associated with $r_b^* = r_b - d = r_a$ in Fig. 6, since r and q are Fourier equivalents.

Generally, power-law scattering, $I(q) \propto q^{-P}$, is found for mass-fractal, surface-fractal or diffuse interfaces. The decay at low q, near a structural limit to fractal scaling, can be described by $I(q) \propto q^{*-P} = \{[\text{erf}\,(qR_g/6^{1/2})]^3/q\}^P$. Since the structural limit is decribed by the same term used in the Guinier expression, R_g, no new terms are introduced by consideration of this limit.

Equations (21)–(23) are restricted to radially symmetric particles. In application to scattering data, the approach is satisfactory for a wide variety of systems (Beaucage & Schaefer, 1994; Beaucage, Ulibarri, Black & Schaefer, 1994; Ulibarri, Beaucage, Sdhaefer, Olivier & Assink, 1992; Hua, Anderson, Hareid, Smith & Beaucage, 1994).

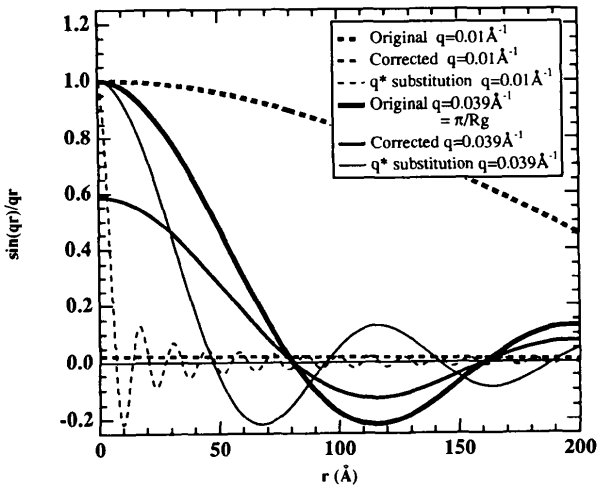

Fig. 7. Comparison between the original function $w(q, r)$, the corrected function and the approximation of equation (22) for $q = \pi/R_g$ and for $q < \pi/R_g$.

5. A unified equation

Guinier's exponential form and the structurally limited power law, discussed above, can be considered independent sources of scattering under the assumption that the structural limit included in q^* accounts for limits to the length of the vector **r** when a local description of the correlation function is no longer applicable. This is an approximation because the structural limit to the power law [(22) and (23)] is an approximate form. The summation of these two components can closely approximate scattering from a wide variety of systems,

$$I(q) = G\exp(-q^2R_g^2/3) + B\{[\text{erf}(qR_g/6^{1/2})]^3/q\}^P, \quad (24)$$

where $G = n^2N_pI_e$ is the exponential prefactor and B is a constant prefactor specific to the type of power-law scattering observed as determined by the regime in which P falls. For Porod's law, $B = 2\pi N_p\rho_e^2S_pI_e$, where $\rho_e = n/V_p$ and S_p is the surface area for the particle.

As noted above, the structurally limited power law does not introduce new parameters since the same parameter that characterizes the exponential decay in scattering, *i.e.* R_g in Guinier's law, also describes the low-q cut-off due to finite-size effects. Equation (24) has been found to be a good approximation for any morphology containing a random distribution of structure (Beaucage & Schaefer, 1994; Hua, Anderson, Hareid, Smith & Beaucage, 1994). Several examples that can be easily calculated are presented later. Specicifically, comparisons are made with calculated scattering patterns from a mass-fractal structure with $d_f = 2$ such as an ideal polymer coil, polydisperse spheres that display Porod behavior and randomly oriented ellipsoids of revolution with a shell of lower scattering density that show power laws steeper than -4.

6. A high-q limit to power-law scattering

Besides a large-size low-q limit to power-law scattering at R_g, as discussed above, many structures are also known to display a small-size high-q limit to the specific mass or surface scaling displayed by a power-law regime. An example of this is shown in Fig. 1 for the power law between $q = 10^{-4}$ to 10^{-2} Å^{-1}. Classic power laws deviate from measured scattering curves at the high-q structural limit. For the case of a mass fractal such as polymer coil, the minimum size to fractal scaling is the average subunit size or the radius of gyration for the persistence length of a polymer chain. For a surface fractal, an equivalent subunit to fractal scaling exists, R_{sub} in Fig. 9. For the case of a surface fractal, the subunit-limiting radius of gyration, R_{sub}, may not coincide with the size of the average structural unit in this scattering regime, R_s. For example, surface-fractal scattering may be limited by surface structures that agglomerate at the surfaces of large particles, R_{sub} (Fig. 9). Within the matrix phase, these subparticulates might not agglomerate, leading to a smaller R_s. It is most general to introduce a new size scale R_{sub} that accounts for possible deviations. This is the only new parameter introduced in this paper. R_{sub} generally is identical to the radius of gyration for the small-scale structure, R_s.

The large-q cut-off for fractal scaling has been previously shown to involve an exponential function as a prefactor to a scattering power law (Guinier & Fournet, 1955, pp. 27–28). This behavior has been known since the 1940s as variations of the exponential form for Guinier's law for different particulate geometries. For example, Guinier & Fournet (1955, pp. 27–28) note that, for randomly oriented thin lamellar discs,

$$\overline{F^2(q)}_{\text{random discs}} \simeq \mathbf{exp}(-\boldsymbol{q^2H^2/3})(2n^2/\boldsymbol{q^2R^2}), \quad (25)$$

where R is the radius of the disc and H is half the thickness. The exponential cut-off and the power law are highlighted in bold in (25). The thickness of the lamellae, $2H$, is the small-size limit (high q) to -2 power-law behavior.

A Guinier-like exponential cut-off at high q for power-law scattering naturally falls out of calculations for power-law scattering from randomly oriented rods and

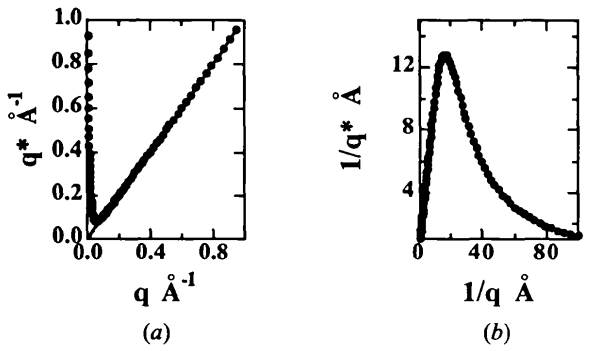

Fig. 8. (*a*) q^* *versus* q and (*b*) $1/q^*$ *versus* $1/q$ showing the difference between the reduced q^* and q.

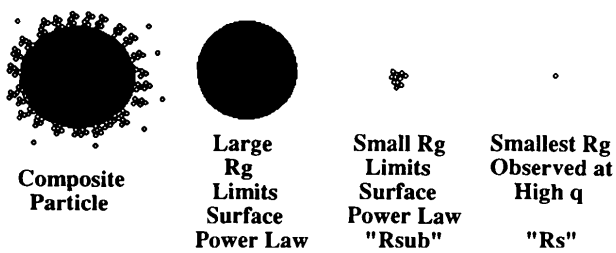

Fig. 9. A typical case in which two R_g's are observed. Particles composed of subparticles where a radius of gyration for the entire particle, R_g, and a radius of gyration for the subparticles, R_s, are observed. The surface-fractal cut-off radius of gyration, R_{sub}, differs from the high-q radius of gyration, R_s, in this case. Generally, $R_s = R_{sub}$.

discs. A Guinier-like cut-off to a surface-fractal scaling regime can also be obtained by analogy to a Debye–Waller factor containing a root-mean-square size that is taken to be R_g. It can also be derived using the arguments for a Guinier exponential form presented in this paper, as described below.

Power-law equations contain a contrast factor such as ρ_e^2 in (23). At large 'r', compared with the substructural size, the contrast is uniform. As 'r' approaches the substructural size, R_s, the uniform contrast breaks down into component elements that have some average structural size, R_s. For q in the power-law regime, the weighting function, $w(q, r)$, of Fig. 2 is constant for these small sizes, so that these structural features are 'averaged out'. When the first oscillations in $w(q, r)$ approach R_s, that is when $2\pi/q$ approaches R_s, power-law scattering due to surface- or mass-fractal structure decays since the conditions for this type of scattering no longer exist. For Porod's law, the surface can no longer be viewed as a sharp interface between homogeneous sources of scattering. A probability function, p_s, is considered that will modify ρ_e^2, in (23), for example. In the derivation of Porod's law, it is cases where the vector **r**'s origin is in the Porod bulk and termination is in the Porod surface that lead to nonoscillatory terms and the q^{-4} dependence in the Fourier transform of the correlation function. Since ρ_e is squared in (23), two independent vectors that lead to this situation must be considered. If the Porod surface is not homogeneous, then there is some probability that the termination points for these two vectors fall in the matrix phase. Two termination points separated by the vector **r** are considered, both points falling in the Porod surface. The probability that both of these points fall in the particle phase of the inhomogeneous surface will modify the power-law function.

For two points, separated by a vector **r**, both in the Porod surface, p_s describes the probability of both points falling in the subparticle phase with the assumption of a random distribution and orientation of the subparticles,

$$p_s(r) \propto \exp(-3r^2/2\sigma^2), \tag{26}$$

where (26) is analogous to (8). As in (10), the squared variance, σ^2, is given by $2R_s^2$, where R_s is the radius of gyration for the subparticles that limit power-law scaling. Equation (26) is Fourier transformed to yield the q-space form that describes an exponential prefactor to ρ_e^2 [in (23), for example]. This exponential cut-off to power-law scattering at high q describes the small-scale structural limit, (27).

$$p_s(q) = \exp(-R_s^2 q^2/3). \tag{27}$$

Superimposed on this exponentially cut-off power-law scattering is the subparticulate Guinier regime that is followed in q space by the substructural power-law regime. These terms contribute to the scattered intensity independently as described below.

7. Extension of the unified equation for multiple structural levels

The two size limits for power-law scattering can be described by an extension of (24) with the high-q exponential cut-off for power-law scattering, (27),

$$\begin{aligned} I(q) \simeq\ & G\exp(-q^2R_g^2/3) \\ & + B\exp(-q^2R_{\text{sub}}^2/3)\{[\text{erf}\,(qR_g/6^{1/2})]^3/q\}^P \\ & + G_s\exp(-q^2R_s^2/3) + B_s\{[\text{erf}\,(qR_g/6^{1/2})]^3/q\}^{P_s}. \end{aligned} \tag{28}$$

For Fig. 9, the first two terms in (28) are analogous to (24) for the large R_g with a high-q power-law cut-off at R_{sub} described by an exponential function, $p_s(q)$, that modifies B. The last two terms in (28) are (24) for the smaller substructure, R_s, with the high-q cut-off for the substructural power law out of the observed size range. In this way, we can describe scattering from a system with interrelated multiple-size-scale features over a very large range of q. Equation (28) will describe the scattering pattern of Fig. 1, for example. It should be noted that although (28) appears cumbersome, no new parameters have been introduced over local fits using Guinier's law and local power laws except for the high-q power limiting radius of gyration, R_{sub}, that usually equals the substructural radius of gyration, R_s.

Equation (28) can be extended to describe an arbitrary number of interrelated structural levels under the generally applicable assumption that $R_{\text{sub}} = R_s$,

$$\begin{aligned} I(q) \simeq \sum_{i=1}^{n}\Big(& G_i\exp(-q^2R_{g_i}^2/3) + B_i\exp(-q^2R_{g_{(i+1)}}^2/3) \\ & \times\{[\text{erf}\,(qkR_{g_i}/6^{1/2})]^3/q\}^{P_i}\Big). \end{aligned}$$

In (29), $i = 1$ refers to the largest-size structural level. Extensions, such as (29), can only be justified when data extend over many decades in q. Again, (29) introduces no new parameters over local Guinier and power-law fits.

8. Results/discussion

Several examples of simple scattering patterns that can be calculated exactly are presented in this section: a mass-fractal structure with mass-fractal dimension 2 such as a polymer coil, polydisperse spheres that display Porod behavior, randomly oriented ellipsoids of revolution with a shell of lower electron density that show power laws steeper than -4, and randomly oriented rod and lamellar systems where morphologies with two structural levels are calculated.

8.1. *Comparison of equation* (24) *and calculations for mass-, surface-fractal and diffuse interfacial scattering*

Scattering from an ideal polymer coil can be described using the Debye equation (Debye, 1947),

$$I(q) = 2A[\exp(-R_g^2q^2) - 1 + (R_g^2q^2)]/(R_g^2q^2)^2. \quad (30)$$

Fig. 10 shows a calculated scattering curve using (30) with $R_g = 50$ Å and $A = 100$ cm^{-1}. By comparison of (24) with the Debye equation, a simple functional relationship between the power-law prefactor, B, the radius of gyration, R_g, of the coil and the experimental prefactor, G, can be obtained:

$$B = 2G/R_g^2 \quad (31)$$

for a Debye coil. A comparison between the unified equation and the Debye equation is quite favorable (Fig. 10). A slight deviation occurs near $q = 0.05$ Å^{-1}. As noted above, this deviation is due to the approximation of substituting q^* for q. The deviation occurs between $q = 2\pi/R_g$ and π/R_g as discussed above. Least-squares fits to the Debye equation yield errors in R_g of about 5% and errors in the prefactor of about 1%. This degree of accuracy is sufficient for most applications. B in the unified equation was fixed at $2G/R_g^2$ according to (30). There are no free parameters in the calculation.

The scattering pattern from a Gaussian distribution of 100 spheres with a median radius of 50 Å and a standard deviation of 10 Å is shown in Fig. 11. The average radius of gyration is 39.5 Å. Porod behavior is expected at high q. The agreement between the calculated scattering curve for polydisperse spheres and that calculated using (24) and the same parameters is quite good. A slight deviation from the calculated curve occurs at about $q = 0.075$ Å^{-1} and leads to errors in R_g and the power law of about 1% in a least-squares fit that is not shown. This deviation is probably due to incomplete averaging of the Fourier peaks in the sphere function.

Scattering from a particle with a diffuse interface can be simulated by calculation of the scattering curve from randomly oriented ellipsoidal particles with a shell of lower electron density. Equation (24) is compared to such

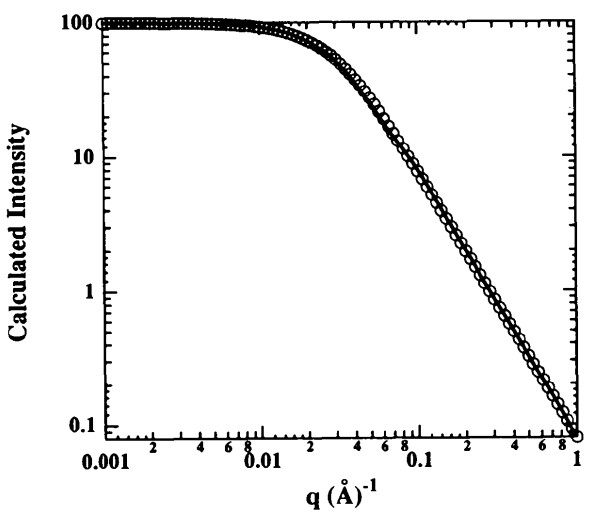

Fig. 10. Log–log plot of Debye equation (○) and equation (24) (solid line). For the Debye equation, $R_g = 50$ Å and $A = 100$ cm^{-1}. For the unified equation, (24), all parameters are fixed. $R_g = 50$ Å, $G = 100$ cm^{-1}, $P = 2$ (the Debye equation represents a mass fractal with $d_f = 2$) and $B = 0.08 = 2G/R_g^2$ from equation (30).

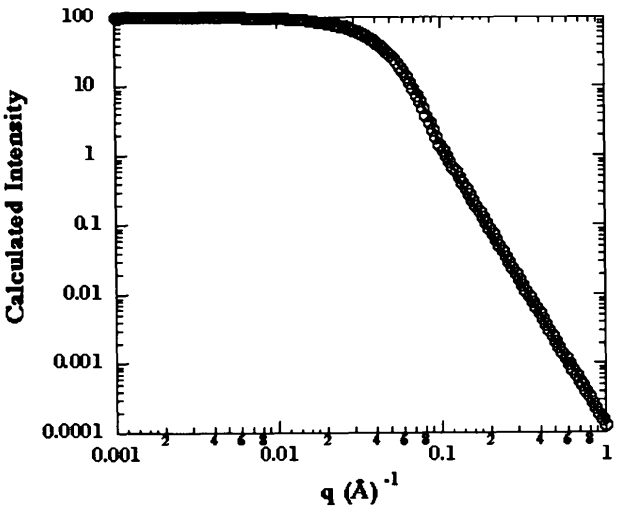

Fig. 11. Calculated scattering (○) from polydisperse spheres with Porod surfaces (power law -4). The solid line follows equation (24) with $R_g = 39.495$ Å as calculated and $P = 4$, $G = 100$ cm^{-1} (fixed in the sphere calculation) and $B = 0.000\,127\,52$ from Porod's law.

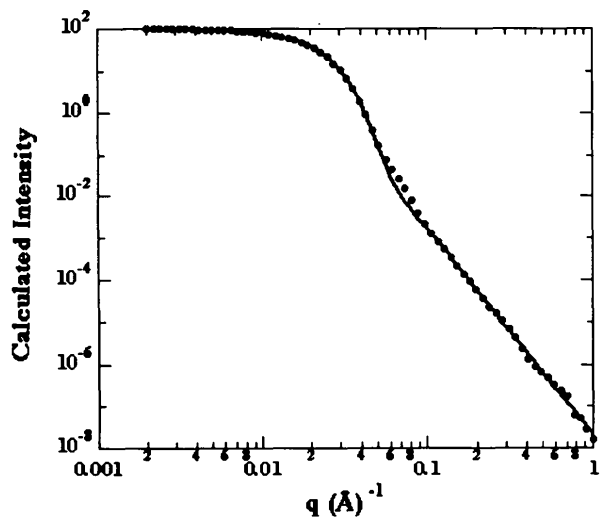

Fig. 12. Calculated scattering curve for an ellipsoid of revolution with a spherical shell of lower electron density, 0.36 of core, with major : minor axis ratio of 4 : 1 and minor axis of $R = 50$ Å and 60 Å for the core and shell, respectively. Equation (24) is calculated using $R_g = 87.9$, $G = 100$ cm^{-1}, $P = 4.91$ and $B = 1.99 \times 10^{-8}$. The mismatch at $q = 0.07$ Å^{-1} is due to a residual Fourier peak that has not been averaged out and that would normally not appear in experimental data for a diffuse interface.

a calculated curve with parameters from local exponential and power-law fits in Fig. 12. The power-law slope in Fig. 12 is close to -5.

Figs. 10, 11 and 12 demonstrate the broad applicability of the unified approach to a diversity of systems. Equation (24) is the first scattering function capable of describing exponential and power-law scattering for mass-, surface-fractal and diffuse interfacial scattering.

8.2. *Comparison of equations* (28) *and* (29) *with calculations for morphologies with two structural levels*

The scattering pattern for randomly oriented thin cylinders and thin lamellar discs can be calculated using an integral equation [Fournet, 1951; Guinier & Fournet, 1955, p. 19, equation (33)]. In both cases a small-scale and a large-scale structural limit serve to delimit a power-law regime. Thin lamellar discs are two-dimensional objects, so that a power law of -2 is expected between the average width of the lamellae and the thickness of the lamellae. Thin rods are one-dimensional objects, so a power law of -1 is expected between the average length of the rods and the average radius of the rods. Equation (28) is compared with these two systems in Figs. 13 and 14. In both cases the high-q oscillations in the calculated curves are due to monodispersity in the small dimension and the failure of the calculation to properly average all orientations. These oscillations are usually absent in experimental data such as those shown in Fig. 1. In both cases, (28) is a good approximation.

Equation (28) has eight parameters, all of which can be independently calculated for rod and lamellar scattering. For the rod calculation, G is fixed at 100 and $R_g^2 = (2H)^2/12 + R^2/2$, where H is half the length of the rod and R is the radius (Feigin & Svergun, 1987, p. 69). B for the power law -1 regime is given by $B = \pi G/(2H)$ (Guinier & Fournet, 1955, pp. 27–28). R_s and R_{sub} are given by $R_s^2 = 3R^2/4$ through a comparison of Guinier's law with equations for rod scattering (Guinier & Fournet, 1955, pp. 27–28). G_s is given by $G(V_p/V_{rod})^2$, where V_p is the volume of a sphere of radius R_s and V_{rod} is the volume of the rod. This relationship between G and G_s is obtained from the definition of the Guinier prefactor. P_s is 4 and B_s is given by Porod's law as $2\pi S\rho_e^2$, that is $2\pi(S/V)G/V$, where S/V is the surface-to-volume ratio. For a rod, S/V is $2/R$. Calculated values are given in the figure captions.

For a lamellar disc, the parameters of (28) can also be calculated. In Fig. 14, G is fixed at 100, $R_g^2 = (2H)^2/12 + R^2/2$, where H is half the thickness of the lamellae and R is the radius (Feigin & Svergun, 1987, p. 69). B for the power-law -2 regime is given by $B = 2G/R^2$ (Guinier & Fournet, 1955, pp. 27–28). R_s and R_{sub} are fixed at H through a comparison of Guinier's law with equations for disc scattering (Guinier & Fournet, 1955, pp. 27–28). G_s is given by $G(V_p/V_{disc})^2$, where V_p is the volume of a sphere of radius H and V_{disc} is the volume of the disc. P_s is 4 and B_s is given by Porod's law as in the rod example. S/V is $1/H$ for a disc. Calculated values are given in the figure caption.

Equations (24), (28) and (29) have been compared with experimental data in previous work (Beaucage & Schaefer, 1994; Beaucage, Ulibarri, Black & Schaefer,

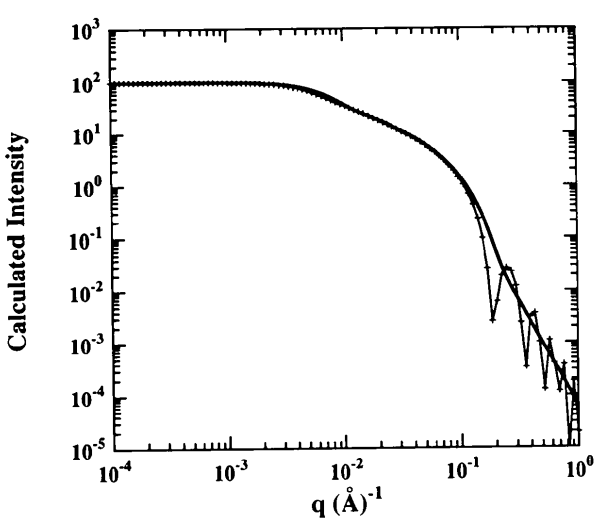

Fig. 13. Calculated scattering curve [Guinier & Fournet, 1955, p. 19, equation (33)] from randomly oriented rods of diameter 40 Å and length 800 Å (+). $I(0)$ is fixed at 100. The calculated scattering curve using equation (28) is shown by the bold line, and $G = 100$, $R_g = 231.4$ Å, $P = 1$, $B = 0.393$, $R_{sub} = R_s = 17.3$ Å, $G_s = 0.111$, $B_s = 6.25 \times 10^{-5}$ and $P_s = 4$ as discussed in the text. High-q oscillations in the + curve are due to poor averaging in the calculation.

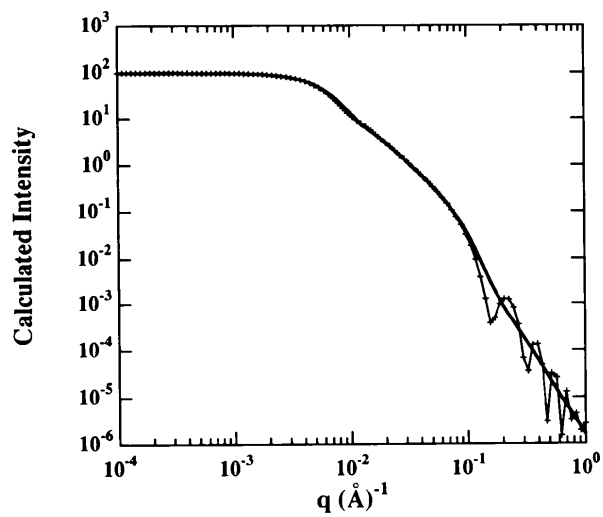

Fig. 14. Calculated scattering curve [Guinier & Fournet, 1955, p. 19, equation (33)] from randomly oriented disc-like lamellae of thickness 40 Å and diameter 800 Å (+). $I(0)$ is fixed at 100. The calculated scattering curve using equation (28) is shown by the bold line, and $G = 100$, $R_g = 283.1$ Å, $P = 2$, $B = 1.25 \times 10^{-3}$, $R_{sub} = R_s = 20$ Å, $G_s = 2.78 \times 10^{-4}$, $B_s = 1.56 \times 10^{-6}$ and $P_s = 4$ as discussed in the text. High-q oscillations in the + curve are due to poor averaging in the calculation.

1994; Ulibarri, Beaucage, Schaefer, Olivier & Assink, 1992; Hua, Anderson, Hareid, Smith & Beaucage, 1994).

9. Concluding remarks

A new approach to the description of small-angle scattering over a wide range of q has been presented. This approach successfully describes scattering from multiple-size-scale structures over q ranges of many orders of magnitude without introducing new parameters other than those used in local fits. The use of the unified equation, presented here, clarifies the range in q over which fits to power law and Guinier's exponential form are applicable since limits to these regimes are included in the function. The unified approach has broad applicability. It is the first model that can simultaneously account for exponential scattering and power-law scattering of arbitrary type, *i.e.* mass-, surface-fractal, Porod or diffuse-interfacial scattering.

The unified approach leads to more accurate values for the power-law slopes and the radius of gyration since a wider range of data is used in the fits and since account is made for the overlap of different scattering regimes. This approach is particularly useful in cases where power laws show weak statistics and when an exponential regime is obscured by low- and high-q power-law scattering.

The author expresses his gratitude to Alan Hurd and Dale Schaefer, both of Sandia National Laboratories, for their detailed reviews and discussions concerning this work. Some of this work was performed under the auspices of the US Department of Energy by Sandia National Laboratories under Contract no. DE-AC04-94AL85000.

References

BEAUCAGE, G. & SCHAEFER, D. W. (1994). *J. Non-Cryst. Solids*, **172–174**, 797–805.

BEAUCAGE, G., ULIBARRI, T. A., BLACK, E. & SCHAEFER, D. W. (1994). In *Organic Hybrid Materials*, edited by J. MARK. American Chemical Society Symposium Series.

DEBYE, P. (1915). *Ann. Phys. (Leipzig)*, **46**, 809–823.

DEBYE, P. (1947). *J. Phys. Colloid. Chem.* **51**, 18–32.

DEBYE, P., HENDERSON, H. R. & BRUMBERGER, H. (1957) *J. Appl. Phys.* **28**, 679–683.

FEIGIN, L. A. & SVERGUN, D. I. (1987). *Structure Analysis by Small-Angle X-ray and Neutron Scattering*. New York: Plenum Press.

FISCHER, M. E. & BURFORD, R. J. (1967). *Phys. Rev.* **156**, 583–622.

FOURNET, G. (1951). *Bull. Soc. Fr. Mineral. Cristallogr.* **74**, 39–113.

GUINIER, A. & FOURNET, G. (1955). *Small-Angle Scattering of X-rays*. New York: Wiley.

HUA, D. W., ANDERSON, J., HAREID, S., SMITH, D. M. & BEAUCAGE, G. (1994). *Better Ceramics through Chemistry* 6, edited by A. K. CHEETHAM, C. J. BRINKER, M. L. MECARTNEY, & C. SANCHEZ, pp. 985. Materials Research Society Proceedings Vol. 346. Pittsburgh, PA: Materials Research Society.

HURD, A. J. (1990). *Optimal Fiber Materials and Processing*, edited by J. W. FLEMING, C. H. SIGEL, S. TAKAHASHI & P. W. FRANCE, p. 3. Materials Research Society Proceedings Vol. 172. Pittsburgh, PA: Materials Research Society.

KORBERSTEIN, J. T., MORRA, B. & STEIN, R. S. (1980). *J. Appl. Cryst.* **13**, 34–45.

LIN, M. Y., KLEIN, R., LINDSAY, H. M., WEITZ, D. A., BALL, R. C. & MEAKIN, P. (1990). *J. Colloid Interface Sci.* **137**, 263–280.

MOUNTAIN, R. D. & MULHOLLAND, G. W. (1988). *Langmuir*, **4**, 1321–1326.

MOUNTAIN, R. D., MULHOLLAND, G. W. & BAUM, H. (1986). *J. Colloid Interface Sci.* **114**, 67–81.

POROD, G. (1951). *Kolloid-Z.* **124**, 83–114.

POROD, G. (1952). *Kolloid-Z.* **125**, 51–57, 109–122.

POROD, G. (1982). *Small-Angle X-ray Scattering*, edited by O. GLATTER, & O. KRATKY, p. 30. London: Academic Press.

SCHAEFER, D. W. & HURD, A. J. (1990). *Aerosol Sci. Tech.* **12**, 876–890.

SCHMIDT, P. W. (1992) *J. Appl. Cryst.* **15**, 567–569.

ULIBARRI, T. A., BEAUCAGE, G., SCHAEFER, D. W., OLIVIER, B. J. & ASSINK, R. A. (1992). *Submicron Multiphase Materials*, edited by R. H. BANEY, L. R. GILLIOM, S. HIRANO & H. K. SCHMIDT, p. 85. Materials Research Society Symposium Proceedings, Vol. 274. Pittsburgh, PA: Materials Research Society.

WILSON, A. J. C. (1949). *X-ray Optics*. New York: Wiley.

WILTZIUS, P., BATES, F. S., DIERKER, S. B. & WIGNALL, G. D. (1987). *Phys. Rev. A*, **36**, 2991–2994.